A JOINT CLASSIFICATION AND SEGMENTATION APPROACH FOR DENDRITIC SPINE SEGMENTATION IN 2-PHOTON MICROSCOPY IMAGES

Ertunc Erdil[⋆] *A. Ozgur Argunsah*[†] *Tolga Tasdizen*[‡⋆] *Devrim Unay*[§] *Mujdat Cetin*[⋆]

[⋆] Faculty of Engineering and Natural Sciences, Sabanci University, Tuzla, Istanbul, Turkey
{ertuncerdil, mcetin}@sabanciuniv.edu
[†] Champalimaud Neuroscience Programme, Champalimaud Centre for the Unknown, Lisbon, Portugal
ali.argunsah@neuro.fchampalimaud.org
[‡]Scientific Computing and Imaging Institute, Department of Electrical and Computer Engineering
University of Utah, Salt Lake City, UT, USA
tolga@sci.utah.edu
[§]Biomedical Engineering Department, Bahcesehir University, Besiktas, Istanbul, Turkey
devrim.unay@eng.bahcesehir.edu.tr

ABSTRACT

Shape priors have been successfully used in challenging biomedical imaging problems. However when the shape distribution involves multiple shape classes, leading to a multimodal shape density, effective use of shape priors in segmentation becomes more challenging. In such scenarios, knowing the class of the shape can aid the segmentation process, which is of course unknown *a priori*. In this paper, we propose a joint classification and segmentation approach for dendritic spine segmentation which infers the class of the spine during segmentation and adapts the remaining segmentation process accordingly. We evaluate our proposed approach on 2-photon microscopy images containing dendritic spines and compare its performance quantitatively to an existing approach based on nonparametric shape priors. Both visual and quantitative results demonstrate the effectiveness of our approach in dendritic spine segmentation.

***Index Terms*—** Dendritic spine segmentation, joint classification and segmentation, multimodal shape density, nonparametric shape priors, active contours, 2-photon microscopy.

1. INTRODUCTION

Dendritic spines are the post-synaptic partners of a synapse. It has been shown that spine structure and function are highly coupled. Dendritic spines have two major components: spine head and spine neck whose sizes affect electrical and chemical compartmentalization. Spine head volume and neck length as well as neck width change through either regular plasticity mechanisms or pathological conditions [1, 2, 3]. Studying such structure requires accurate segmentation of spines, whose shapes belong to one of several classes.

In the literature, spines are generally grouped into three classes: mushroom, thin, and stubby. However, a coarser level classification of spine shapes reveals two spine classes: spines that have a neck (mushroom and thin) and those that do not (stubby) [4]. Stubby spines consist of only a head and can be segmented using intensity and context information. Segmentation of spines that have a neck is a more challenging problem, because the area containing the spine neck generally has very low contrast and is blurry in 2-photon microscopy images. Therefore, prior knowledge about spine neck is required for successful segmentation.

In the literature, several techniques have been proposed for spine segmentation in 2-photon microscopy images. Thresholding based methods such as [5, 6] suffer from the difficulty of finding an appropriate threshold. Since the intensity level of neck is generally very low, it is usually not possible to find a threshold that segments the spine with its neck. The main bottleneck of all existing methods in the literature is that they use only intensity information for segmentation. Therefore, they cannot be easily used for segmentation of spines from different classes.

In this paper, we propose an approach for joint classification and segmentation of spines from different classes in 2-photon microscopy images. First, our approach segments the spine head using an intensity-based active contour method proposed by Chan and Vese [7], coupled with some contextual information about the spine head in the region of interest (ROI). After spine head segmentation, the class of the spine to be segmented is inferred using the features of the spatial intensity distribution in parts of the image that are likely to contain a potential spine neck. These areas are determined by utilizing information about the location of the segmented head. The segmentation process terminates for spines that are classified as stubby. For spines that have necks, the segmentation process continues using statistical prior information about spine necks, based on manually segmented training images of spines with necks. In particular, we use the nonparametric shape priors method of Kim et al. [8] for spine neck segmentation.

The first, broad contribution of our work is that, to the best of the authors' knowledge, this is the first time any kind of shape prior has been used for segmenting dendritic spines from microscopic images. The second, more specific contribution of our approach is that it involves joint segmentation and classification of spines. In particular, partial segmentation information is used to infer the spine shape class, which in turn is exploited to refine and finalize the segmentation process. This approach effectively handles the multimodal shape distribution while exploiting prior information about intensity distributions in the potential neck region. Using the nonparametric

This work has been supported by the Scientific and Technological Research Council of Turkey (TUBITAK) under Grant 113E603 and by a TUBITAK-2221 Fellowship for Visiting Scientists and Scientists on Sabbatical Leave.

shape priors approach of Kim et al. [8] directly on the original problem turns out to be insufficient, whereas it can be effectively used in our framework in the neck segmentation phase after classification. Our experimental results demonstrate the effectiveness of our approach.

2. PROPOSED APPROACH

In this section, we present our joint classification and segmentation approach for dendritic spine segmentation in 2-photon microscopy images. Our approach consists of three stages: spine head segmentation, classification, and spine neck segmentation.

2.1. Spine Head Segmentation

Our approach takes a region of interest (ROI) containing the spine as input. We assume that the spine head is located around the center of the ROI and the ROI is rotated such that the neck is roughly perpendicular to the horizontal axis as shown in Figure 1(a). In our experiments, we perform the ROI selection and rotation manually. However, in practice, the ROI can be selected automatically using an automatic spine detection approach [9]. Automatic rotation of the ROI can in practice be performed by exploiting information about the location of the dendrite, provided by a dendrite segmentation approach [10].

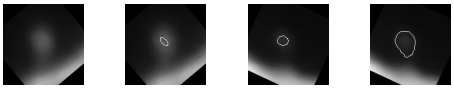

(a) (b) (c) (d)

Fig. 1. (a) A sample ROI, (b) an initial curve, (c) and (d) spine head segmentations with $\mu = 1$ and $\mu = 0.5$, respectively

For spine head segmentation, we use active contours with the energy function proposed by Chan and Vese [7] coupled with some contextual information about the location of the spine head. Using the assumption that the spine head is located around the center of the ROI, we multiply the image intensities with a 2D circular Gaussian function - $G_\sigma(x, y)$, with a standard deviation of σ - such that the center of the Gaussian corresponds to the center of the ROI. This indicates a preference for finding a spine head in the center of the ROI. Based on this perspective, we use the following energy functional:

$$E(C) = \lambda_1 \oint_C ds + \lambda_2 \Big(\int_{inside(C)} G_\sigma(x,y).|I_0(x,y) - c_1|^2 dxdy + \int_{outside(C)} G_\sigma(x,y).|I_0(x,y) - \mu.c_2|^2 dxdy \Big) \quad (1)$$

where, C is the evolving curve, I_0 is image to be segmented, c_1 and c_2 are the average intensities, respectively inside and outside C. The first term is the *curve length penalty* which produces smooth curves using the assumption that shorter curves are statistically more likely than longer ones. λ_1 and λ_2 are constants and we fix $\lambda_1 = \lambda_2 = 1$ in our experiments.

The curve evolution starts with an initial curve as shown in Figure 1(b). We use the narrowband representation of the level set function in curve evolution. The narrowband representation and the context information represented by the constant $G_\sigma(x, y)$ in Eq.1 prevents the inclusion of the dendrite in the foreground region. We fix $\sigma = 10$ in our experiments.

Note that another deviation from the original Chan-Vese approach is that we multiply c_2 in the energy function with a constant $\mu \in (0, 1)$. This is to allow the spine head boundary to move towards the dendrite. Not having this factor keeps the spine head boundary too far away from the dendrite due to the large intensities of the dendrite region. Segmentation results without such weighting (i.e., $\mu = 1$), and with the weighting we use in our experiments ($\mu = 0.5$) are shown in Figure 1(c) and 1(d), respectively.

2.2. Classification

In order to segment the neck region, we need prior information about neck shapes, as it is hard to make further progress solely based on the intensities of the test image. However that information depends on the spine class (namely with or without neck). Hence, by exploiting the spine head, segmented as described in Section 2.1, in this section we propose an approach for inferring the spine class. Our training set consists of image intensities as well as the associated manual head and neck segmentations of 18 spines (see Figure 2). 12 of those are mushroom spines (which have a neck) and 6 are stubby spines (which do not have a neck).

If the spine neck exists, it is located in the area below the spine head. Therefore, once we have the spine head segmentation, we can find the location of the potential spine neck easily. This motivates us to infer the spine class based on image intensities in the regions where the neck might appear. First, we grab a rectangular region such that the bottom point of the spine head (shown by a red cross in Figure 3(a)) lies at the center of the rectangle. The second rectangular region shown in Figure 3(b) is drawn such that it is located just below the spine head. We fix size of the first and second rectangles to 40×110 and 10×130, respectively, in a 150×150 ROI. Using these two rectangular regions, we construct three sets of feature vectors from the training set for classification. The first set of feature vectors are obtained by summing up the intensities in the first rectangle horizontally. Similarly, the second set of feature vectors are obtained by vertical summation of the intensities in the same rectangle. We present the statistics of these two feature vectors extracted from the training set for each class in Figure 4(a) and 4(b). In these figures, error bars indicate one standard deviation around the mean. The final set of feature vectors are the histograms of intensities in the second rectangular region. We present average of these histograms for each spine class in Figure 4(c). Visual inspection of these feature vectors suggest that they contain discriminatory information about the spine class.

(a) First region (b) Second region

Fig. 3. Regions where a potential neck is likely to be contained in.

We design a linear-kernel support vector machines (SVM) classifier based on each feature vector. Given a test image with a segmented spine head, we run each classifier. We infer the spine class based on majority voting on the outputs of the three classifiers. We observe that using the three classifiers provides better results than using any two of them. Rather than performing decision fusion, one might also consider concatenating the feature vectors towards a single classifier.

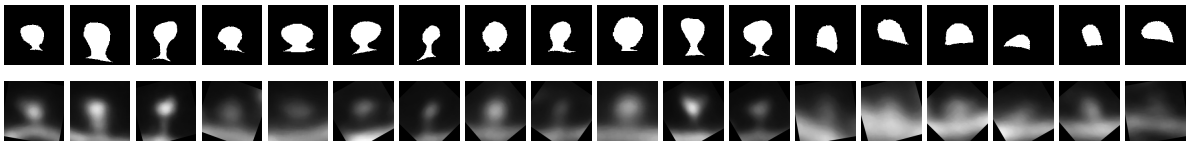

Fig. 2. Training set containing examples from both mushroom and stubby classes. First row: Manual segmentations of expert. Second row: Corresponding intensity images of the manual segmentations in the first row.

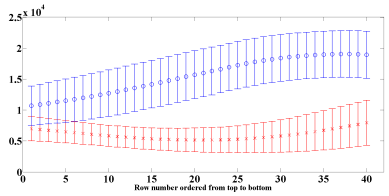

(a) Statistics (mean $\pm$ one standard deviation) of the first feature vector based on training data.

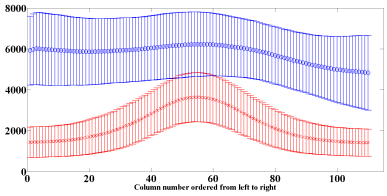

(b) Statistics (mean $\pm$ one standard deviation) of the second feature vector based on training data.

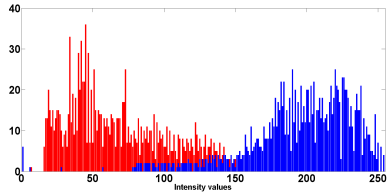

(c) Mean of the third feature vector based on training data.

Fig. 4. Visualization of different set of feature vectors. Red indicates the spines that have a neck. Blue indicates spines without necks.

The segmentation process terminates for the spines classified as stubby (without a neck). Otherwise, the segmentation process continues with the spine neck segmentation step which is introduced in the next subsection.

2.3. Spine Neck Segmentation

In this section, we describe the final stage of the segmentation process of the spines classified as having a neck. In particular, we evolve the spine boundary found by the approach described in Section 2.1 further by using nonparametric shape priors [8], where the prior information about the neck part comes from expert neck segmentations in our training data, shown in Figure 5. Neck shapes in the training set are already aligned. A training set of overall spine shapes (head and neck) are obtained by adding each spine neck in the training set to the spine head already found in previous stage (see Figure 5). Hence we do not seek to modify the head piece further in this stage.

We use the following energy function for neck segmentation with shape priors:

$$E(C) = \alpha\Big(\int_{inside(C)} |I_0(x,y) - c_1|^2 dxdy + \int_{outside(C)} |I_0(x,y) - c_2|^2 dxdy\Big) - \beta \log(p_C(C)) \quad (2)$$

where, $p_C(C) = \frac{1}{n}\sum_{i=1}^{n} k(d_{L_2}(\phi_C, \phi_i), \sigma)$ is the learned shape prior density, $k(.,\sigma)$ is a 1D Gaussian kernel with kernel size σ, $d_{L_2}(.,.)$ is the L_2 distance metric, n is the number of training shapes, and ϕ_C and ϕ_i are the level set representations of the evolving curve C and the i^{th} shape in the training set, respectively. The constants α and β control the contribution of each term to curve evolution and we set $\alpha = 0.1$ and $\beta = 5$. Note that the weight α on the data fidelity term is relatively small. This mainly reflects the perspective that (1) head segmentation has already been achieved, and (2) most of the information about the neck will come from the training data. The role of the data fidelity term at this stage is mainly to ensure a coherent integration of the head and the neck piece.

	Proposed Method	Kim et al.	Chan and Vese
Spine 1	0.8303	0.8389	0.1737
Spine 2	0.7426	0.6744	0.0000
Spine 3	0.7140	0.6619	0.2636
Spine 4	0.7291	0.6386	0.2658
Spine 5	0.8426	0.6221	0.2996
Spine 6	0.8095	0.7678	0.2036
Spine 7	0.8618	0.7282	0.5671
Spine 8	0.8021	0.7516	0.1783
Spine 9	0.8927	0.8469	0.1133
Spine 10	0.8333	0.8141	0.6339
Spine 11	0.8291	0.7388	0.5032
Spine 12	0.8482	0.7846	0.4157
Spine 13	0.7886	0.7990	0.4357
Spine 14	0.7868	0.7045	0.1517
Spine 15	0.8892	0.8450	0.3891
Spine 16	0.7599	0.7500	0.4863
Spine 17	0.8135	0.7322	0.4501
Spine 18	0.4156	0.4820	0.2017
Spine 19	0.7876	0.9244	0.1977
Spine 20	0.6839	0.7383	0.1906
Spine 21	0.7753	0.8068	0.3243
Spine 22	0.7727	0.8566	0.2020
Average	0.7822	0.7375	0.3021

Table 1. Quantitative evaluation of segmentation accuracy through the Dice coefficient. Spines from Spine 1 to 17 have necks, the remaining ones do not.

Given the limited role of the data term, we simply use the basic Chan-Vese data term here.

We keep evolving the curve with the gradient flow of the energy function given in Eq. (2) until it converges.

3. EXPERIMENTAL RESULTS

The experiments are conducted on 22 spines different from the ones used in the training set. We evaluate the performance of our segmentation method with respect to manual delineations of a domain expert using the Dice coefficient [11]. We also obtain Dice coefficient results for the methods presented by Chan and Vese [7] and Kim et al. [8]. The original method by Kim et al. performs segmentation based on a shape prior density estimated from the entire spine training shapes shown in Figure 2.

We present a quantitative analysis of our segmentation results in Table 1. Our joint segmentation and classification approach achieves

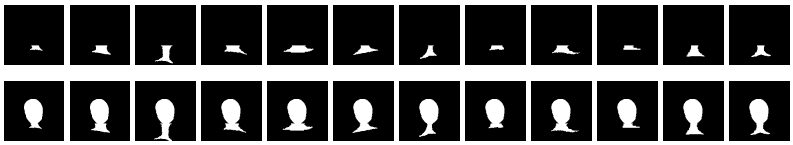

Fig. 5. First row: aligned training set of spine neck shapes. Second row: training set of spine shapes constructed after spine head segmentation. Note that the spine neck segmentations in the first row belong to the first 12 spines in Figure 2.

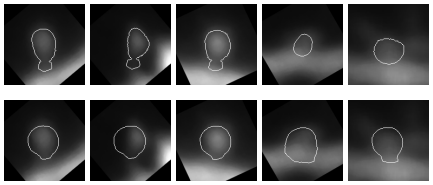

Fig. 6. Visual segmentation results on Spine 1, Spine 4, Spine 15, Spine 18, and Spine 22 from left to right. First row: proposed method. Second row: Kim et al.

the best results in terms of the Dice coefficient. Comparison of the results of our approach with those of Kim et al. and Chan and Vese based on a paired t-test provides statistical significance levels of $p = 0.069$ and $p = 0.5 \times 10^{-12}$, respectively. We note that adapting and applying the nonparametric shape priors approach of Kim et al. to the spine segmentation problem would itself be a contribution, yet we improve the performance of that approach further by our joint classification and segmentation strategy. Our classification approach classifies all spines except Spine 12 correctly. We should also point out that we have explored several ways of using nonparametric shape priors in the post-classification segmentation phase of our approach (such as exploiting the class information and then evolving the entire spine boundary using the corresponding head or head+neck training shapes). While these ideas have provided some improvements over Kim et al.'s original approach, we have achieved the most significant improvements using the approach described in Section 2.3.

Some visual segmentation results are presented in Figure 6. Although, average Dice coefficient results of the two methods are close to each other, our approach provides significantly better visual segmentation results, due to its success in capturing the challenging neck region.

4. CONCLUSION

We have proposed a joint classification and segmentation approach for dendritic spine segmentation in 2-photon microscopy images. These images are more challenging than corresponding confocal microscopy images, however, they are useful for analyzing the temporal evolution of spines. Our approach infers the class of the spine to be segmented during the segmentation process and adapts the remaining steps of the segmentation process accordingly. Our experimental study suggests that this is an effective strategy for exploiting prior information about the shapes and intensities of spines that belong to different classes.

Our current study is limited to two coarse spine classes: those with and without a neck. Our examples came from spines labeled as mushroom (with a neck) and stubby (without a neck). One could extend our study to include other defined spine shapes such as thin and filopodia, and identify more classes. Furthermore, one could also consider subdividing these defined classes into subclusters based on learned features from the training data and exploit that information in the segmentation phase as well. Another line of work could be to extend our approach to 3D spine volumes. One might also consider building a similar approach on a different shape representation than level sets.

5. REFERENCES

[1] A. Govindarajan, I. Israely, S. Y. Huang, and S. Tonegawa, "The dendritic branch is the preferred integrative unit for protein synthesis-dependent ltp," *Neuron*, vol. 69, no. 1, pp. 132–146, 2011.

[2] M. F. Bear, K. M. Huber, and S. T. Warren, "The mglur theory of fragile x mental retardation," *Trends in neurosciences*, vol. 27, no. 7, pp. 370–377, 2004.

[3] S. M. Weng, F. McLeod, M. E. S. Bailey, and S. R. Cobb, "Synaptic plasticity deficits in an experimental model of rett syndrome: long-term potentiation saturation and its pharmacological reversal," *Neuroscience*, vol. 180, pp. 314–321, 2011.

[4] E. A. Nimchinsky, B. L. Sabatini, and K. Svoboda, "Structure and function of dendritic spines," *Annual review of physiology*, vol. 64, no. 1, pp. 313–353, 2002.

[5] W. Bai, X. Zhou, L. Ji, J. Cheng, and S. T. C. Wong, "Automatic dendritic spine analysis in two-photon laser scanning microscopy images," *Cytometry Part A*, vol. 71, no. 10, pp. 818–826, 2007.

[6] J. Cheng, X. Zhou, E. Miller, R. M. Witt, J. Zhu, B. L. Sabatini, and S. T. C. Wong, "A novel computational approach for automatic dendrite spines detection in two-photon laser scan microscopy," *Journal of neuroscience methods*, vol. 165, no. 1, pp. 122–134, 2007.

[7] T. F. Chan and L. A. Vese, "Active contours without edges," *IEEE Transactions on Image processing*, vol. 10, no. 2, pp. 266–277, 2001.

[8] J. Kim, M. Çetin, and A. S. Willsky, "Nonparametric shape priors for active contour-based image segmentation," *Signal Processing*, vol. 87, no. 12, pp. 3021–3044, 2007.

[9] L. Rada, E. Erdil, A. O. Argunsah, D. Unay, and M. Cetin, "Automatic dendritic spine detection using multiscale dot enhancement filters and sift features," *IEEE International Conference on Image Processing*, 2014.

[10] A. Greenblum, R. Sznitman, P. Fua, P. E. Arratia, M. Oren, B. Podbilewicz, and J. Sznitman, "Dendritic tree extraction from noisy maximum intensity projection images in c. elegans," *Biomedical engineering online*, vol. 13, no. 1, pp. 74, 2014.

[11] L. R. Dice, "Measures of the amount of ecologic association between species," *Ecology*, vol. 26, no. 3, pp. 297–302, 1945.